COMPUTATIONAL MATHEMATICS
BANACH CENTER PUBLICATIONS, VOLUME 13
PWN—POLISH SCIENTIFIC PUBLISHERS
WARSAW 1984

NUMERICAL SOLUTION OF INITIAL-VALUE PROBLEMS IN PLASMA PHYSICS*

JOHN KILLEEN

Magnetic Fusion Energy Computer Center,
Lawrence Livermore National Laboratory,
University of California,
Livermore, California 94550

1. Introduction

Numerical calculations have had an important role in controlled fusion research since its beginning in the early 1950's, but the application of computers to plasma physics has advanced rapidly in the last few years. One reason for this is the increasing sophistication of the mathematical models of plasma behavior, and another is the increased speed and memory of the computers which made it reasonable to consider numerical simulation of plasmas.

The behavior of a plasma confined by a magnetic field is simulated by a variety of numerical models. Some models used for short times give detailed knowledge of the plasma on a microscopic scale, while other models used for much longer times compute macroscopic properties of the plasma dynamics. All of these models are under continual development, and in the next few years there will be a substantial increase in the use of numerical models in order to meet the needs of the fusion power program.

Prior to 1973, research in computational plasma physics primarily consisted of calculations with particle codes used to simulate collisionless plasmas. The primary emphasis of these studies is to contribute to the understanding of plasma theory, particularly velocity space instabilities and wave-particle interactions. In order to simulate fusion devices computational plasma physicists are now developing many new macroscopic codes. Equilibrium, magnetohydrodynamic, and Tokamak transport codes

* Work performed under the auspices of the U. S. Department of Energy by Lawrence Livermore National Laboratory under contract No. W-7405-Eng-48.

have already given much insight into the understanding of experimental results, and have aided in the design of future reactors.

For the purpose of discussing the physical models, and also the numerical methods, it is convenient to consider the following categories of computer codes used to model the physics of fusion devices.

1. Time-dependent magnetohydrodynamics.
2. Plasma transport in a magnetic field.
3. MHD and guiding-center equilibria.
4. MHD stability of confinement systems.
5. Vlasov and particle models.
6. Multi-species Fokker–Planck codes.
7. Hybrid codes.

In a short paper it is impossible to review all of the above topics, so a brief description will be given of two of the categories, followed by some examples.

1.1. Time-dependent magnetohydrodynamics. Detailed comparison of experimental data from pulsed high-beta devices with theory, taking due account of experimental complications depends on the application of 2-D and 3-D (two- and three-dimensional) versions of codes analogous to the 1-D Hain–Roberts code [1]. Most of the physical phenomena important here lie in the fast MHD time scale (nanoseconds to microseconds). For tokamak configurations, the corresponding effects occur on longer time scales-milliseconds; however, the questions of stability of Tokamak discharges toward MHD modes are very important. One example of great interest is the study of the early stages of a Tokamak discharge and the formation and destruction of magnetic surfaces. Here also the relevant times are on the fast MHD time scale.

The article by Roberts and Potter [2] gives a good review of the role of MHD computations and discusses methods for the solution of time-dependent problems. I have also written a review article for *Information Processing* 71 which considers both time-dependent and time-independent [3] problems. Recent research in this area is described in three review papers ([4], [5], and [6]).

There are a great variety of MHD codes being developed. Within the fluid theory various degrees of complexity are considered. The so-called ideal MHD is an infinite conductivity approximation. The more realistic models include the transport coefficients, e.g., thermal conductivity and electrical resistivity, and these can be scalars or tensors ([1], [7]). Two-dimensional codes are now fairly standard and there are several three-dimensional codes. In some cases perturbation theory is used and the equations are then linearized and Fourier analyzed in one or two coordinates.

The choice of coordinate system varies among these codes. A fixed Eulerian grid is the usual choice, but Lagrangian descriptions, particularly using magnetic flux surfaces as coordinate surfaces [5], are proving useful in certain problems as are particle-in-cell methods [8]. In the work of Brackbill [4] a moving grid is used which is not a Lagrangian grid.

A variety of difference schemes are being used, ranging from fully explicit using a Lax–Wendroff or a leap-frog scheme, to implicit methods employing the ADI scheme or "splitting" (the method of fractional time steps). In a later section of this paper we shall describe the application of implicit difference methods to problems in resistive magnetohydrodynamics.

1.2. Multi-species Fokker–Planck codes. In the simulation of magnetically confined plasmas where the ions are not Maxwellian and where a knowledge of the distribution functions is important, kinetic equations must be solved. At number densities and energies typical of mirror machines, the end losses are due primarily to the scattering of charged particles into the loss cones in velocity space by classical Coulomb collisions. The kinetic equation describing this process is the Boltzmann equation with Fokker–Planck collision terms [9]. The use of this equation is not restricted to mirror systems. The heating of plasmas by energetic neutral beams, the thermalization of α-particles in DT plasmas, the study of runaway electrons and ions in Tokamaks, and the performance of two-energy component fusion reactors are other examples where the solution of the Fokker–Planck equation is required [10].

The problem is to solve a nonlinear partial differential equation for the distribution function of each charged species in the plasma, as functions of seven independent variables (three spatial coordinates, three velocity coordinates, and time). Such an equation, even for a single species, exceeds the capability of any present computer so several simplifying assumptions are therefore required to treat the problem. In the final section of this paper we shall discuss the solution to the Fokker–Planck equations in a two-dimensional velocity space and the coupling to a spatially dependent Tokamak transport code.

Resistive magnetohydrodynamics

In order to achieve the high densities and temperatures required for a successful fusion reactor, a plasma must be confined by a magnetic field for a sufficiently long time. In the attempts to achieve this confinement, the problem of stability has emerged as one of the most important. The most dangerous types of instabilities are the magnetohydrodynamic (MHD) instabilities in which the plasma is assumed to

behave as a conducting fluid and the instabilities involve displacement of macroscopic portions of the plasma. It is a particular MHD instability, the resistive instability which is considered in this paper.

Resistivity can destroy the stabilization achieved by the shearing of the lines of force. In the case of a magnetic field which has shear or which changes direction, the magnetic energy can be reduced by allowing the fields to mix and annihilate. This is prevented by a perfectly conducting plasma, but with finite conductivity an instability can develop in which the magnetic lines of force are torn into "islands". This type of resistive instability is known as a resistive tearing mode [11].

There are three types of resistive modes: (1) the rippling mode, which is driven by a gradient in the resistivity and is usually not important when large temperature gradients are unlikely; (2) the gravitational mode (g-mode) which is the resistive equivalent of the interchange instability and is important in sheared systems; and (3) the tearing mode, which is the resistive equivalent of the kink mode and involves displacement of the whole plasma.

The modes grow on a time scale intermediate between the resistive diffusion time $\tau_R = 4\pi a^2/\eta c^2$ and the hydromagnetic transit time $\tau_H = a(4\pi\varrho)^{1/2}B^{-1}$ where a is a characteristic dimension of the plasma layer, η is the resistivity, ϱ is the mass density of the plasma, B is the magnetic field, and c is the speed of light.

The resistive instability of an incompressible plasma was first systematically investigated by Furth, Killeen, and Rosenbluth [11]. They used the plane slab model, in which the equilibrium depends only on y, the magnetic field is $\hat{x}B_{x_0} + \hat{z}B_{z_0}$, and $\vec{v}_0 = 0$. In that paper perturbations of the form $f_1(y)\exp[i(k_x x + k_z z) + \omega t]$ are assumed, and the problem is to solve an eigenvalue problem for ω, the growth rate of instability. In order to solve the problem the plasma is divided into two regions, a narrow inner region about the plane for which the wave vector is perpendicular to the zero-order magnetic field ($\vec{k}\cdot\vec{B}_0 = 0$) and an outer region where the infinite conductivity equations hold. By matching the solutions within the resistive layer to the outer ideal MHD solutions, FKR found resistive tearing modes with growth rates, $p = \omega\tau_R$, proportional to $S^{2/5}$, where $S = \tau_R/\tau_H$.

Due to the many possible equilibrium configurations and the many approximations necessary to make the problem analytically tractable, it is usually not possible to analytically describe the general parameter dependence of the growth rates. In order to obtain results for specific and wide choices of equilibrium magnetic fields and boundary conditions, numerical models have been developed to study these resistive instabilities.

In this paper we assume an arbitrary time-dependence and the problem becomes an initial-value problem. Two regions are not used, i.e., the same equations hold throughout the plasma. The initial-value problem is then solved numerically. This method of solution was developed ([12]) for the linear model simultaneously with the analytic technique and is described in [13]. The initial-value codes, RIPPLE, use the same basic equations and assumptions as FKR and are capable of finding tearing, rippling, and gravitational modes as well as mixed modes.

In order to consider more realistic equilibrium magnetic fields, a cylindrical model, RIPPLE IV, was developed ([13]), which also used the equations of incompressible magnetohydrodynamics. This model has been extensively applied to the study of tearing modes in reversed field pinch ([14]–[18]), and tokamak ([18]) equilibria. Dibiase developed a new cylindrical model ([18], [19]) which includes the effects of compressibility, viscosity, and thermal conductivity along with finite resistivity. This model has also been applied to the RFP ([15]–[20]).

Recently there has been interest in the effect of equilibrium flow on the tearing mode ([21]–[22]). We have developed a new linear initial-value code, RIPPLE V ([22]), to study this problem. For this work we have gone back to the plane slab model using the incompressible MHD equations.

We have also applied the linear slab model to the double tearing mode ([24]). In this case there are two neighboring singular surfaces, i.e., surfaces for which $\vec{k}\cdot\vec{B}_0 = 0$. If these surfaces lie close to one another, the modes at each singular surface may interact leading to an enhanced growth rate.

In all of the above linear models the initial-value problems solved are one-dimensional, i.e., the zero-order fields are given by $\vec{B}_0(y)$ or $\vec{B}_0(r)$ and the perturbed variables take the form

$$f_1(y, t)\exp[i(k_x x + k_z z)] \quad \text{or} \quad f_1(r, t)\exp[i(m\theta + k_z z)].$$

In many toroidal confinement devices it is not possible to specify the equilibrium fields as functions of one variable. In tokamaks and other axisymmetric toroidal devices the zero-order field can be specified by $\vec{B}_0(r, z)$. To study tearing modes in such configurations we have developed a new two-dimensional, linear code, RIPPLE VI, ([23]) in which the perturbations are of the form $f_1(r, z, t)\exp[in\varphi]$, $n \geqslant 1$. We use the incompressible MHD equations to derive a set of eight coupled linear partial differential equations. For the case, $n = 0$, we have developed a 2D axisymmetric linear code (ALIMO), which makes use of field and velocity stream functions, resulting in a system of four equations.

The above linear models are discussed in more detail in Section 2.1 of this paper. These codes are used for extensive parameter studies of prospective equilibria. Stable and unstable regions of wave number space, growth rates of exponentially growing modes and their mode structure are calculated. In order to study the longtime, large amplitude behavior of these modes, and to simulate experimental devices in controlled fusion research, the non-linear fluid equations must be solved. In general, such a calculation requires the simultaneous advancement in time of eight non-linear partial differential equations in several spatial dimensions.

As discussed above, one of the effects of non-vanishing resistivity is the occurance of unstable modes which have no counterpart in ideal MHD theory ([11]). These resistive instabilities grow on time scales which can be long relative to the fastest time scales of the system, leading to severe computational problems. Recently, the evolution and interaction of these modes in tokamaks has been successfully and extensively studied ([25]–[29]) by assuming an ordering that eliminates the fastest time scales from the problem and results in a reduced set of equations for the scalar flux and stream functions ([30]). This allows the calculation to proceed rapidly for the large values of S, the magnetic Reynolds number, typical of tokamak discharges. However, certain effects, such as those due to finite plasma pressure, are exluded. These effects can be important in controlled fusion devices, such as Reversed Field Pinches and High Beta Tokamaks.

In Section 3 we describe a two-dimensional, non-linear, resistive MHD model ([31], [32]) which retains all the normal modes of the system. It is general in that the equations are cast in orthogonal curvilinear coordinates, making calculations in a variety of coordinate systems possible. For certain cases, the model employs a transformation to helical coordinates which allows the solution of the three-dimensional equations under the assumption that helical symmetry is preserved. We present the mathematical model in which the relevant equations are expressed as a set of conservation laws. Computational techniques for the solution of these equations are discussed. The boundary conditions, including the important case of singular boundaries, are considered. Examples of the non-linear evolution of tearing modes ([33]) and resistive g-modes ([34]) for the Reversed Field Pinch are published.

2. Linear calculations

2.1. Basic equations and assumptions. We assume that the hydromagnetic approximation is valid, and the ion pressure and inertia terms are neglected in Ohm's law. An isotropic resistivity is assumed, the fluid

is assumed to be incompressible, and perturbations in resistivity result only from convection. The basic equations are:

$$\frac{\partial \vec{B}}{\partial t} = \operatorname{curl}(\vec{v} \times \vec{B}) - \operatorname{curl}\left(\frac{\eta}{4\pi} \operatorname{curl} \vec{B}\right), \tag{2.1}$$

$$\operatorname{div} \vec{B} = 0, \quad \operatorname{div} \vec{v} = 0, \tag{2.2}$$

$$\operatorname{curl}\left(\varrho \frac{d\vec{v}}{dt}\right) = \operatorname{curl}\left(\frac{1}{4\pi} \operatorname{curl} \vec{B} \times \vec{B}\right), \tag{2.3}$$

$$\frac{\partial \eta}{\partial t} + \vec{v} \cdot \nabla \eta = 0. \tag{2.4}$$

In equations (2.1)–(2.3) we consider $\vec{B} = \vec{B}_0 + \vec{B}_1$ and $\vec{v} = \vec{v}_0 + \vec{v}_1$, where $\vec{B}_0$ and $\vec{v}_0$ are given and the subscript 1 denotes perturbed quantities. We obtain, to first order, the following set of linearized equations:

$$\frac{\partial \vec{B}_1}{\partial t} = \operatorname{curl}(\vec{v}_0 \times \vec{B}_1 + \vec{v}_1 \times \vec{B}_0) - \frac{1}{4\pi} \operatorname{curl}(\eta_0 \operatorname{curl} \vec{B}_1 + \eta_1 \operatorname{curl} \vec{B}_0), \tag{2.5}$$

$$\operatorname{div} \vec{B}_1 = 0, \quad \operatorname{div} \vec{v}_1 = 0, \tag{2.6}$$

$$\varrho_0 \operatorname{curl}\left[\frac{\partial \vec{v}_1}{\partial t} + (\vec{v}_0 \cdot \nabla)\vec{v}_1\right] = \frac{1}{4\pi} \operatorname{curl}[(\vec{B}_0 \cdot \nabla)\vec{B}_1 + (\vec{B}_1 \cdot \nabla)\vec{B}_0]. \tag{2.7}$$

2.2. Effect of equilibrium flow on the tearing mode. The resistive tearing instability of an incompressible plasma is investigated for the plane sheet pinch in which the equilibrium magnetic field, $\hat{x}B_{x_0} + \hat{z}B_{z_0}$, depends only on y. The effect of a non-zero v_0 is studied. For a symmetric magnetic equilibrium and modes $a = a(k_x^2 + k_z^2)^{1/2} < 1$ an exponential growth develops. The growth rate, $p = \omega\tau_R$, is computed as a function of a and $S = \tau_R/\tau_H$, for several values of v_0. The effect is to reduce p for all a, and to reduce the marginal a for instability for values of v_0 of the order of the resistive diffusion velocity. For asymmetric tearing, the effect of the diffusion velocity depends on its sign. The velocity may have either a stabilizing or destabilizing influence on both the growth rates and the critical a for instability ([22]).

From equations (2.5)–(2.7), a pair of equations can be separated which involve only B_{y_1} and v_{y_1}. The remaining quantities are not needed for the analysis of tearing modes. We define the following parameters $a = ka$, $k = (k_x^2 + k_z^2)^{1/2}$, $v = v_0\tau_R/a$ where $\vec{v}_0 = \hat{y}v_0$. We now define the dimensionless variables, $\mu = y/a$, $\tau = t/\tau_R$, $\psi = B_{y_1}/B$, $w = -iv_{y_1}k\tau_R$, $\eta = \dfrac{\eta_0}{\langle\eta\rangle}$, $\theta = -\dfrac{i\eta_1}{\langle\eta\rangle}$ and define $F = (1/kB)(k_x B_{x_0} + k_z B_{z_0})$. We

have

$$\frac{\partial \psi}{\partial \tau} = \eta\left[\frac{\partial^2 \psi}{\partial \mu^2} - a^2\psi\right] - Fw - \nu\frac{\partial \psi}{\partial \mu} + aF'\theta, \tag{2.8}$$

$$\frac{1}{a^2S^2}\frac{\partial}{\partial \tau}\left[\frac{\partial^2 w}{\partial \mu^2} - a^2 w\right] = -\frac{\nu}{a^2S^2}\frac{\partial}{\partial \mu}\left[\frac{\partial^2 w}{\partial \mu^2} - a^2 w\right] + \tag{2.9}$$

$$+F\left[\frac{\partial^2 \psi}{\partial \mu^2} - a^2\psi\right] - F''\psi.$$

A difference equation corresponding to (2.8) is obtained by a Crank–Nicholson scheme. Equation (2.9) is differenced as follows:

$$\frac{1}{a^2S^2\Delta\tau}[(\delta^2 w)_j^{n+1} - a^2 w_j^{n+1} - (\delta^2 w)_j^n + a^2 w_j^n] \tag{2.10}$$

$$= -\frac{\nu}{2a^2S^2}[(\delta^3 w)_j^{n+1} + (\delta^3 w)_j^n] +$$

$$+\frac{\nu}{4S^2\Delta\mu}(w_{j+1}^{n+1} - w_{j-1}^{n+1} + w_{j+1}^n - w_{j-1}^n) - \tfrac{1}{2}F_j''(\psi_j^{n+1} + \psi_j^n) +$$

$$+\tfrac{1}{2}F_j[(\delta^2\psi)_j^{n+1} - a^2\psi_j^{n+1} + (\delta^2\psi)_j^n - a^2\psi_j^n].$$

The symbol $(\delta^2\psi)_j^n$ denotes the usual second divided difference of ψ at the point $(j\Delta\mu, n\Delta\tau)$, while $(\delta^3 w)_j^n$ denotes the third divided difference of w which is correct to second order and is spread over four mesh widths. We can use either free space or conducting wall boundary conditions on ψ and w ([22]).

The implicit nature of the difference scheme involves solving a large linear system of equations at each time step. This system can be expressed as $M\vec{u}^{n+1} = \vec{z}^n$, where $\vec{u}^{n+1} = (\ldots, \psi_j^{n+1}, w_j^{n+1}, \ldots)$ and z^n contains the known values ψ_j^n, w_j^n. Since none of the coefficients in (2.8) and (2.9) vary in time, neither does M. At the start of each run after M is generated, it is decomposed via Gaussian elimination into a product of a lower and an upper triangular matrix, $M = LU$. The matrices LU are stored over M, and at each time step we need only solve two triangular systems by back substitution.

2.3. Cylindrical models. The linear model given by equations (2.5)–(2.7) can be applied in cylindrical geometry in order to study specific diffuse pinch configurations. The equilibrium is given by $\vec{B}_0(r) = \hat{\theta}B_{\theta_0}(r) + \hat{z}B_{z_0}(r)$, $\vec{v}_0 = 0$, and $\eta_0 = \eta_0(r)$. These functions are chosen to describe a particular experiment, and the stabilizing effect of the location of the conducting walls (R_w) with reference to the singular surface can be determined.

We assume perturbations of the form $f_1(r,t)\exp[i(m\theta+k_z z)]$. We can find a consistent system of four equations involving the components $B_{r_1}, B_{\theta_1}, v_{r_1}, v_{\theta_1}$ and an equation for η_1. These equations are solved by an initial-value code, RIPPLE IV, using numerical methods analogous to those of the previous sections.

This code has been applied to the study of tearing modes in reversed field pinch equilibria ([14], [18]). An analytic example of such an equilibrium is the Bessel Function Model (BFM) given by $B_{\theta_0} = J_1(r)$ and $B_{z_0} = J_0(r)$. The effects of viscosity and compressibility on these modes can also be studied with the cylindrical code, RESTAB ([19]).

2.4. Toroidal model, $n \neq 0$. In axisymmetric toroidal devices, such as tokamaks with non-circular minor cross-section, the zero-order fields can be specified by

$$\vec{B}_0 = \hat{r}B_{r_0}(r,z) + \hat{\varphi}B_{\varphi_0}(r,z) + \hat{z}B_{z_0}(r,z). \tag{2.11}$$

To study tearing modes in such configurations we have developed a linear code, RIPPLE VI, in which the perturbations are of the form $f_1(r,z,t)\times$ $\times\exp[in\varphi]$.

In equations (2.5)–(2.7), we consider the case where $\vec{v}_0 = 0$, $\eta_1 = 0$, and $\eta_0 =$ constant. Equations (2.5) and (2.6) then yield four equations for $B^R_{r_1}, B^I_{r_1}, B^R_{z_1}, B^I_{z_1}$ where the superscripts denote the real and imaginary parts of the complex perturbations. The equation for $B^R_{z_1}$ is typical

$$\frac{\partial B^R_{z_1}}{\partial t} = \frac{\eta_0}{4\pi}L(B^R_{z_1}) + B_{r_0}\frac{\partial v^R_{z_1}}{\partial r} - B_{\varphi_0}\frac{n}{r}v^I_{z_1} + B_{z_0}\frac{\partial v^R_{z_1}}{\partial z} - \frac{\partial B_{z_0}}{\partial r}v^R_{r_1} - \frac{\partial B_{z_0}}{\partial z}v^R_{z_1} \tag{2.12}$$

where

$$L(u) = \frac{1}{r}\frac{\partial}{\partial r}\left(r\frac{\partial u}{\partial r}\right) - \frac{n^2}{r^2}u + \frac{\partial^2 u}{\partial z^2}. \tag{2.13}$$

As in previous sections we take the curl of equation (2.7) and use equation (2.6) to obtain

$$-\varrho_0\frac{\partial}{\partial t}(\nabla^2\vec{v}_1) = \frac{1}{4\pi}\mathrm{curl}\,\mathrm{curl}[(\vec{B}_0\cdot\nabla)\vec{B}_1 + (\vec{B}_1\cdot\nabla)\vec{B}_0]. \tag{2.14}$$

Equation (2.14) yields four equations for $v^R_{r_1}, v^I_{r_1}, v^R_{z_1}, v^I_{z_1}$. The eight equations can be summarized in the following

$$\frac{\partial B^R_{r_1}}{\partial t} = f_1(B^R_{r_1}, B^R_{z_1}, v^R_{r_1}, v^R_{z_1}, v^I_{r_1}), \tag{2.15a}$$

$$\frac{\partial B_{z_1}^R}{\partial t} = f_2(B_{z_1}^R, v_{r_1}^R, v_{z_1}^R, v_{z_1}^I), \tag{2.16a}$$

$$\frac{\partial}{\partial t}\left[L(v_{r_1}^R) + \frac{2}{r}\frac{\partial v_{r_1}^R}{\partial r} + \frac{v_{r_1}^R}{r^2} - \frac{2}{r}\frac{\partial v_{z_1}^R}{\partial z}\right] = f_3(B_{r_1}^R, B_{r_1}^I, B_{z_1}^R, B_{z_1}^I), \tag{2.17a}$$

$$\frac{\partial}{\partial t}[L(v_{z_1}^R)] = f_4(B_{r_1}^R, B_{r_1}^I, B_{z_1}^R, B_{z_1}^I). \tag{2.18a}$$

The operator L is defined in equation (2.13) and the functions f_i are functions of the first-order variables indicated and their derivatives, as well as functions of the zero-order variables (not shown). Additional equations (2.15b)–(2.18b) for the imaginary components are similar to (2.15a)–(2.18a). Equations (2.17) and (2.18) are non-standard in form and f_3, f_4 involve derivatives up to third order in r and z.

The initial-value problem given by equations (2.15)–(2.18) is solved by implicit finite-difference methods as in previous sections. In the ($\eta_0 =$ constant) case that we are considering, equation (2.16ab) does not contain B_{r_1}, so we first solve for $B_{z_1}^R, B_{z_1}^I$ implicitly using $v_{r_1}^R, v_{z_1}^R, v_{z_1}^I$ from the preceding time step. We then solve equation (2.15ab) in a similar manner but using the new B_{z_1}. The velocity equations (2.17ab) and (2.18ab) are then solved separately implicitly using time-centered difference equations, analogous to (2.10), making use of the predicted B_{r_1}, B_{z_1} already computed from (2.15ab) and (2.16ab). Since the eight equations are solved separately, we provide for a correction cycle using the new velocities in (2.15ab) and (2.16ab) and then the corrected fields in (2.17ab) and (2.18ab). The correction cycle can then be iterated to satisfy a convergence criterion. In practice the correction cycles have not been needed.

The code, RIPPLE VI, has been tested using the one-dimensional equilibria, $\vec{B}_0(r)$, described in the preceding section. The equilibria tested were the Bessel Function Model, the Pitch and Pressure Model ([35]), and the Peaked Tokamak Model ([36]). Tearing mode parameter studies of these models have been run ([4], [8]) with the RIPPLE IV code and good agreement was obtained with earlier results.

2.5. Toroidal model, $n = 0$. The axisymmetric linear MHD code, ALIMO, treats the special case $n = 0$, i.e. where the perturbations are of the form $f_1(r, z, t)$. It is convenient to express the zero-order fields as

$$\vec{B}_0(r, z) = \hat{r}\left(-\frac{1}{r}\frac{\partial \psi_0}{\partial z}\right) + \hat{\varphi}B_{\varphi_0} + \hat{z}\left(\frac{1}{r}\frac{\partial \psi_0}{\partial r}\right) \tag{2.19}$$

where B_{φ_0} and ψ_0 are given, and ψ_0 is the usual poloidal flux function. In equations (2.5)–(2.7) we consider the case where $\vec{v}_0 = 0$, $\eta_1 = 0$, but η_0 is not necessarily constant. The field and velocity perturbations are

expressed by

$$\vec{B}_1(r, z, t) = \hat{r}\left(-\frac{1}{r}\frac{\partial\psi}{\partial z}\right) + \hat{\varphi}B_{\varphi_1} + \hat{z}\left(\frac{1}{r}\frac{\partial\psi}{\partial r}\right), \tag{2.20}$$

$$\vec{v}_1(r, z, t) = \hat{r}\left(-\frac{1}{r}\frac{\partial\varphi}{\partial z}\right) + \hat{\varphi}v_{\varphi_1} + \hat{z}\left(\frac{1}{r}\frac{\partial\varphi}{\partial z}\right) \tag{2.21}$$

where ψ, φ are the perturbed poloidal flux function and velocity stream function, respectively. Equations (2.5)–(2.7) yield the following

$$\frac{\partial\psi}{\partial t} = \frac{\eta_0}{4\pi}\Delta^*\psi - \frac{1}{r}\left(\frac{\partial\psi_0}{\partial z}\frac{\partial\varphi}{\partial r} - \frac{\partial\psi_0}{\partial r}\frac{\partial\varphi}{\partial z}\right), \tag{2.22}$$

$$\frac{\partial B_{\varphi_1}}{\partial t} = \frac{1}{4\pi}\left[\frac{\partial}{\partial r}\left(\frac{\eta_0}{r}\frac{\partial(rB_{\varphi_1})}{\partial r}\right) + \frac{\partial}{\partial z}\left(\eta_0\frac{\partial B_{\varphi_1}}{\partial z}\right)\right] - \tag{2.23}$$

$$-\frac{1}{r}\left[\frac{\partial\psi_0}{\partial z}\frac{\partial v_{\varphi_1}}{\partial r} - \frac{\partial\psi_0}{\partial r}\frac{\partial v_{\varphi_1}}{\partial z} - \frac{\partial\psi_0}{\partial z}\frac{v_{\varphi_1}}{r} + \frac{\partial B_{\varphi_0}}{\partial z}\frac{\partial\varphi}{\partial r} - \left(\frac{\partial B_{\varphi_0}}{\partial r} - \frac{B_{\varphi_0}}{r}\right)\frac{\partial\varphi}{\partial z}\right],$$

$$\frac{\partial v_{\varphi_1}}{\partial t} = \frac{1}{4\pi\varrho_0 r}\left[-\frac{\partial\psi_0}{\partial z}\frac{\partial B_{\varphi_1}}{\partial r} + \frac{\partial\psi_0}{\partial r}\frac{\partial B_{\varphi_1}}{\partial z} - \frac{\partial\psi_0}{\partial z}\frac{B_{\varphi_1}}{r} + \right. \tag{2.24}$$

$$\left. + \frac{\partial B_{\varphi_0}}{\partial z}\frac{\partial\psi}{\partial r} - \left(\frac{\partial B_{\varphi_0}}{\partial r} + \frac{B_{\varphi_0}}{r}\right)\frac{\partial\psi}{\partial z}\right],$$

$$\frac{\partial(\Delta^*\varphi)}{\partial t} = \frac{1}{4\pi\varrho_0 r}\left[-\frac{\partial\psi_0}{\partial z}\frac{\partial(\Delta^*\psi)}{\partial r} + \frac{\partial\psi_0}{\partial r}\frac{\partial(\Delta^*\psi)}{\partial z} + \right. \tag{2.25}$$

$$+\frac{2}{r}\frac{\partial\psi_0}{\partial z}\Delta^*\psi - \frac{\partial(\Delta^*\psi_0)}{\partial r}\frac{\partial\psi}{\partial z} + \frac{\partial(\Delta^*\psi_0)}{\partial z}\frac{\partial\psi}{\partial r} + \frac{2}{r}\Delta^*\psi_0\frac{\partial\psi}{\partial z} +$$

$$\left. + 2r\left(B_{\varphi_0}\frac{\partial B_{\varphi_1}}{\partial z} + \frac{\partial B_{\varphi_0}}{\partial z}B_{\varphi_1}\right)\right]$$

where

$$\Delta^*\psi = r\frac{\partial}{\partial r}\left(\frac{1}{r}\frac{\partial\psi}{\partial r}\right) + \frac{\partial^2\psi}{\partial z^2}. \tag{2.26}$$

The numerical scheme used to solve equations (2.22)–(2.25) is analogous to that of the preceding section. Equations (2.22) and (2.23) are solved implicitly for ψ^{n+1}, $B_{\varphi_1}^{n+1}$ using φ^n and $v_{\varphi_1}^n$. These predicted values of ψ^{n+1} and $B_{\varphi_1}^{n+1}$ are then used in time-centered implicit difference equations for equations (2.24)–(2.25), in order to obtain φ^{n+1} and $v_{\varphi_1}^{n+1}$. Equations (2.22)–(2.23) can then be solved again using a time-centered scheme

to obtain corrected values of ψ^{n+1}, $B_{\varphi_1}^{n+1}$, which are then used to solve equations (2.24)–(2.25) once more.

ALIMO has also been applied to the BFM equilibrium discussed in Section 2.3.

3. Nonlinear calculations

3.1. Mathematical model. As described in Section 2, the resistive MHD equations relate the electromagnetic fields $\vec{E}$ and $\vec{B}$ to the fluid velocity $\vec{v}$ and the thermodynamic variables (the pressure p, the mass density ϱ, and the specific internal energy e). They may be combined into a set of conservation laws for the magnetic flux density $\vec{B}$, the fluid momentum density $\varrho\vec{v}$, the mass density ϱ, and the total energy density $u = \varrho v^2 + B^2 + \varrho e$. In order to make our model applicable to a variety of coordinate systems, we assume a metric of the form $ds^2 = h_1^2 dx_1^2 + h_2^2 dx_2^2 + h_3^2 dx_3^2$, where x_1, x_2, and x_3 are orthogonal curvilinear coordinates with scale factors $h_i = h_i(x_1, x_2)$. Then the relevant equations may be written as

$$\frac{\partial B^i}{\partial t} = \frac{1}{h_1 h_2 h_3} \frac{\partial}{\partial x^k} (h_1 h_2 h_3 \sigma^{ik}), \tag{3.1}$$

$$\frac{\partial(\varrho v^i)}{\partial t} = \frac{-1}{h_1 h_2 h_3} \frac{\partial}{\partial x^k} (h_1 h_2 h_3 \tau^{ik}) + \tau^{nk} \begin{Bmatrix} i \\ nk \end{Bmatrix}, \tag{3.2}$$

$$\frac{\partial \varrho}{\partial t} = \frac{-1}{h_1 h_2 h_3} \frac{\partial}{\partial x^k} (h_1 h_2 h_3 \varrho v^k), \tag{3.3}$$

$$\frac{\partial u}{\partial t} = \frac{-1}{h_1 h_2 h_3} \frac{\partial}{\partial x^k} (h_1 h_2 h_3 f^k), \tag{3.4}$$

where σ^{ik} are the contravariant components of the antisymmetric tensor $\boldsymbol{S} = \vec{B}\vec{v} - \vec{v}\vec{B} + \frac{\eta}{S}(\nabla\vec{B} - \nabla\vec{B}^{\dagger})$, τ^{ik} are the contravariant components of the symmetric tensor $\boldsymbol{T} = \varrho\vec{v}\vec{v} - \vec{B}\vec{B} + \frac{1}{2}(p + B^2)\boldsymbol{I}$, ϱv^k are the contravariant components of the momentum, f^k are the contravariant components of the energy flux $\vec{F} = (u+p)\vec{v} + (B^2\boldsymbol{I} - 2\vec{B}\vec{B})\cdot\vec{v} + \frac{2\eta}{S}(\vec{B}\cdot\nabla\vec{B} - \nabla\vec{B}\cdot\vec{B})$, $S = \tau_R/\tau_H$ and we have invoked the summation convention. The Christoffel symbols appearing in (3.2) arise because of the dependence of the unit vectors on the coordinates, and are defined as in Morse and Feshbach [37].

As discussed in Section 2, the unstable eigenmodes of a cylindrical plasma are in general functions of (r, θ, z). To describe these perturbations in our non-linear code, we must reduce the dimensionality of the problem from three to two. This is accomplished by applying the coordinate transformation $\varphi = m\theta + k_z z$ to the fully three-dimensional equations. The equations in this coordinate system have been detailed elsewhere [33].

3.2. Computational techniques. Our basic equations form a set of Eulerian conservation laws in two spatial dimensions. When finite difference approximations are introduced it proves convenient to do so in such a way as to maintain the conservation properties of the original differential equation. Appropriate spatial difference approximations for scalar (3.3), (3.4) and vector (3.2) conservation laws are obtained in a straightforward manner by the application of Gauss' law to a computational cell. To obtain a conservative scheme for a pseudovector conservation law, $\partial\vec{w}/\partial t = \nabla \times \vec{G}$ (e.g., (3.1)), we must apply Stokes' theorem. We introduce temporal differencing by means of the Alternating Direction Implicit (ADI) method. The final set of difference equations may then be written as

$$\left[1 - \frac{\Delta t}{2}(D_1 + S)\right] \boldsymbol{U}^{n+1/2} = \left[1 + \frac{\Delta t}{2}(D_2 + D_{12} + S)\right] \boldsymbol{U}^n, \tag{3.5}$$

$$\left[1 - \frac{\Delta t}{2}(D_2 + S)\right] \boldsymbol{U}^{n+1} = \left[1 + \frac{\Delta t}{2}(D_1 + D_{12} + S)\right] \boldsymbol{U}^{n+1/2}, \tag{3.6}$$

where $\boldsymbol{U}^n$ represents the state of the system at time t_n, D_i is a finite difference operator in the ith coordinate direction, D_{12} represents the mixed derivatives, and S represents the Christoffel symbols.

Since the operators discussed above are in general non-linear, each step of the ADI algorithm represents a set of $M \times J$ (where M is the length of U and J is the number of mesh points in one direction) non-linear algebraic equations to be solved on each row of the mesh. These equations must be linearized and solved iteratively. We write $(fg)^{(l)} = \frac{1}{2} f^{(l-1)} g^{(l)} + g^{(l-1)} f^{(l)}$ where $f^{(l-1)}$ and $g^{(l-1)}$ are considered as coefficients in the first and second terms, respectively. When equations (3.5)–(3.6) are linearized in this manner, the resulting system is block tridiagonal, and may be written in the form

$$-\boldsymbol{A}_{i,j}^{(l-1)} \cdot \boldsymbol{U}_{i+1,j}^{(l)} + \boldsymbol{B}_{i,j}^{(l-1)} \cdot \boldsymbol{U}_{i,j}^{(l)} - \boldsymbol{C}_{i,j}^{(l-1)} \cdot \boldsymbol{U}_{i-1,j}^{(l)} = \boldsymbol{D}_{i,j}, \quad i = 2, 3, \ldots, I-1 \tag{3.7}$$

subject to the boundary conditions

$$\boldsymbol{G}_1 \cdot \boldsymbol{U}_{1,j}^{(l)} = \boldsymbol{H}_1 \cdot \boldsymbol{U}_{2,j}^{(l)} + \boldsymbol{J}_1 \quad \text{and} \quad \boldsymbol{G}_I \cdot \boldsymbol{U}_{I,j}^{(l)} = \boldsymbol{H}_I \cdot \boldsymbol{U}_{I-1,j}^{(l)} + \boldsymbol{J}_I \tag{3.8}$$

at the left-hand boundary, and at the right-hand boundary respectively. (3.7) may be solved by the well-known algorithm $\boldsymbol{U}_{i,j}^{(l)} = \boldsymbol{E}_i \cdot \boldsymbol{U}_{i+1,j}^{(l)} + \boldsymbol{F}_i$ where $\boldsymbol{E}_i$ and $\boldsymbol{F}_i$ are defined recursively in terms of the boundary conditions. A similar solution can be defined when periodic boundary conditions are imposed. In that case $\boldsymbol{U}_{i,j}^{(l)} = \boldsymbol{E}_i \cdot \boldsymbol{U}_{i+1,j}^{(l)} + \boldsymbol{S}_i \cdot \boldsymbol{U}_{J-1}^{(l)} + \boldsymbol{F}_i$ where $\boldsymbol{E}$, $\boldsymbol{S}$, and $\boldsymbol{F}$ are also determined recursively. Further details may be found in [32].

Once the solution has been advanced to a new time level, the coefficients appearing in (3.7) are updated and the procedure is repeated until the solution converges to within a given tolerance. The time step is adjusted according to the number of iterations required for convergence. If convergence cannot be achieved within a specified number of iterations, the time step is decreased. Conversely, if the solution converges rapidly, the time step is increased. Thus the code always uses the largest possible time step to maintain the desired accuracy.

3.3. Boundary conditions. The boundary conditions on field ($\vec{B}$) and flow ($\vec{v}$) variables at a perfectly conducting boundary are well known. For the thermodynamic variables ϱ and u, we have found it convenient in some cases to impose boundary conditions which require that mass and energy be conserved. For example, if x_2 is taken as the coordinate normal to the wall, a scalar density is advanced according to

$$\frac{\partial \varrho_J}{\partial t} = \frac{2}{(h_1 h_2 h_3)_J \Delta_- x_{2_J}} (h_1 h_3 F_2)_{J-1/2}^{n+1}.$$

For example, the finite difference approximation to the continuity equation (where $F_2 = \varrho v_2$) is $-C(\varrho v_2)_J^{n+1} + \varrho_J^{n+1} = C(\varrho v_2)_{J-1}^{n+1} + \varrho_J^n$, with $C = \Delta t (h_1 h_3)_{J-1/2} / (h_1 h_2 h_3)_J (\Delta_- x_2)_J$. The coefficients appearing in this equation become elements in the boundary condition matrices $\boldsymbol{G}$ and $\boldsymbol{H}$.

The problem of numerically advancing the solution at the origin of coordinates ($r = 0$) is a difficult one, for unless symmetry conditions exist there is no natural boundary condition to be imposed at this point. For instabilities characterized by azimuthal mode number $m = 0$, we can pose the problem in (r, z) cylindrical coordinates. In this case we can apply a modification of the conservative boundary conditions discussed above, where axial fluxes are included in a straightforward manner. When $m^2 > 0$ no axial symmetry exists; one of the independent variables is an angle (θ), and the origin represents the same point in space for all values of this coordinate.

Scalar quantities, such as ϱ and u, must have unique values on axis for any direction of approach, i.e., as we are near $r = 0$ on any ray $\theta =$ constant, these quantities must approach the same limiting value. In polar and helical coordinates this is also the case for B_z and ϱv_z. Evolutionary

equations for such quantities may be found by integrating the appropriate equation over a small cylindrical cell of radius $\Delta r/2$, yielding the equation

$$\frac{\partial u_0}{\partial t} = \frac{-2}{\pi \Delta r} \sum_i \Delta\theta_i F_{i,3/2}.$$

The ADI method decouples the spatial mesh by proceeding in partial time steps, so that on the partial step in which radial terms are treated explicitly, this equation can be used directly. On the other partial step, F must be treated implicitly, thus coupling the solution for all rays (lines for which θ-constant) at $r = 0$. This difficulty is avoided by noticing that F will in general be non-linear and will contain derivatives of u. After linearization and discretization, we can write

$$F^{n+1}_{i,3/2} = P_i u^{n+1}_{i,2} + Q_i u^{n+1}_0 + R_i.$$

The coupling is now removed by reordering the recursive solution on the interior of the mesh as

$$u^{n+1}_{i,j} = e_{i,j} u^{n+1}_{i,j-1} + f_{i,j}, \qquad j = 2, 3, \ldots, J \tag{3.9}$$

i.e., we define the solution from "left to right", instead of "right to left". We then arrive at

$$u^{n+1}_0 = \left\{1 + \frac{\Delta t}{\pi \Delta r} \sum_i \Delta\theta_i (P_i e_{i,2} + Q_i)\right\}^{-1} \cdot \left\{u^n_0 - \frac{\Delta t}{\pi \Delta r} \sum_i \Delta\theta_i (P_i f_{i,2} + R_i)\right\} \tag{3.10}$$

as the expression for the scalar u at the origin. The complete solution is thus obtained by sweeping all rays from the outer boundary to the origin to determine $e_{i,j}$ and $f_{i,j}$ recursively for $j = j-1, j-2, \ldots, 2$, applying (3.10) and then using (3.9) to obtain the interior solution.

When $m^2 > 1$, we know that components of vector quantities must vanish at the origin. However, modes with $m = 1$ are characterized by gross motion across the origin, and we use the uniqueness of the cartesian components to advance vector quantities at $r = 0$. The general form for the equation describing the evolution of a vector quantity is

$$\frac{\partial \vec{V}}{\partial t} = -\frac{1}{r}\frac{\partial}{\partial r}(r\vec{F}) - \frac{1}{r}\frac{\partial \vec{G}}{\partial \theta} - \frac{\partial \vec{H}}{\partial z} + \vec{C} - Vf$$

where $\vec{F}, \vec{G}$, and $\vec{H}$ are the vector fluxes of $\vec{V}$, and $\vec{C}$ represents possible Christoffel terms. We assume that the Cartesian representation of $\vec{V}$ can be obtained by the transformation $\vec{V}_c = a \cdot \vec{V}$. Then the Cartesian

components of $\vec{V}$ evolve according to the equation

$$(3.11)\quad \frac{\partial \vec{V}_c}{\partial t} = -\frac{1}{r}\frac{\partial}{\partial r}(r\boldsymbol{a}\cdot\vec{F}) - \frac{1}{r}\frac{\partial}{\partial \theta}(\boldsymbol{a}\cdot\vec{G}) - \frac{\partial}{\partial z}(\boldsymbol{a}\cdot\vec{H}) + \frac{\partial \boldsymbol{a}}{\partial z}\cdot\vec{H} - \boldsymbol{a}\cdot\nabla f$$

where we have assumed $\boldsymbol{a}$ to be independent of r, and have used $\boldsymbol{a}\cdot\vec{G} = -(1/r)\,\partial\boldsymbol{a}/\partial\theta\cdot\vec{G}$ which, indeed, serves as a definition of $\vec{G}$. When transformation to helical coordinates is performed, equation (3.11) becomes

$$(3.12)\quad \frac{\partial \vec{V}_c}{\partial t} = -\frac{1}{r}\frac{\partial}{\partial r}(r\boldsymbol{a}\cdot\vec{F}) - \frac{1}{r}\frac{\partial}{\partial \varphi}[\boldsymbol{a}\cdot(\vec{G}+rk_z\vec{H})] + k_z\frac{\partial \boldsymbol{a}}{\partial \theta}\cdot\vec{H} - \boldsymbol{a}\cdot\nabla f$$

which points out the reason for allowing $\boldsymbol{a}$ to depend explicitly on the z coordinate. Proceeding in a manner similar to that used for scalar quantities we arrive at the equation

$$\frac{\partial \vec{V}_c}{\partial t} = -\frac{2}{\pi \Delta r}\sum_i \Delta\theta_i \boldsymbol{a}_i\cdot\vec{W}_{i,3/2}$$

where $\vec{W} = \vec{F} - k_z \Delta r\,\boldsymbol{A}\cdot\vec{H}/4 + (\Delta r/4)\nabla f$, and we have used the fact that, for polar coordinates, $\partial\boldsymbol{a}/\partial\theta = \boldsymbol{a}\cdot\boldsymbol{A}$ where $A_{rs} = (-1)^r(1-\delta_{rs})$, $r, s = 1, 2$. A self-consistent solution can now be defined in a manner analogous to that previously described. When we use the linearization $\vec{W}^{n+1}_{i,3/2} = \boldsymbol{P}_i\cdot\vec{V}^{n+1}_{i,2} + \boldsymbol{Q}_i\cdot\vec{V}^{n+1}_{c_0} + \vec{R}_i$ we arrive at $\vec{V}^{n+1}_{c_0} = (\boldsymbol{I}+\boldsymbol{S})^{-1}\cdot(\vec{V}^{n}_{c_0} - \boldsymbol{T})$ where $\boldsymbol{I}$ is the identity matrix, and

$$\boldsymbol{S} = \frac{\Delta t}{\pi \Delta r}\sum_i \Delta\theta_i \boldsymbol{a}_i\cdot[\boldsymbol{P}_i\cdot\boldsymbol{E}_{i,2}\cdot\boldsymbol{a}_i^{-1} + \boldsymbol{Q}_i],$$

$$\boldsymbol{T} = \frac{\Delta t}{\pi \Delta r}\sum_i \Delta\theta_i \boldsymbol{a}_i\cdot[\boldsymbol{P}_i\cdot\vec{F}_{i,2} + \vec{R}_i].$$

The polar components are then obtained by inverting the transformation for each ray, and the interior solution is then found as described previously.

4. Fokker–Planck/Transport model for beam driven Tokamaks

Neutral beam heated Tokamaks [38] are characterized by a warm Maxwellian background plasma, whose evolution can be described by a set of macroscopic transport equations, and one or more energetic species which are quite non-Maxwellian, whose evolution should be represented

by Fokker–Planck equations. The coupling of these systems is by means of particle and energy sources in the multispecies transport equations and a Maxwellian target plasma in the multispecies Fokker–Planck equations.

The Fokker–Planck/Transport (FPT) Code [39] models the time-dependent behavior of such a system. The model assumes the existence of an arbitrary number of Maxwellian warm ion species which are described by their individual densities $n_a(\varrho, t)$ and by a common temperature profile $T_i(\varrho, t)$ where ϱ is the average radius of a flux surface. The electrons are described by a separate temperature profile $T_e(\varrho, t)$ and their density is determined by quasineutrality. The energetic species are represented by velocity space distribution functions $f_b(v, \theta, \varrho, t)$, where v is speed and θ is pitch angle. Since the magnetic flux surface shapes will tend to change more slowly than the macroscopic plasma parameters, it is a valid approximation to allow the transport and collision processes to proceed through a sequence of magnetohydrodynamic equilibria. The poloidal flux ψ, which determines the radial coordinate ϱ, is thus obtained from Ampere's law.

4.1. Fokker–Planck equations. We assume that the distribution functions are azimuthally invariant in velocity space (about the direction of the magnetic field). This assumption reduces the velocity space from three to two dimensions.

The Fokker–Planck collision term for an inverse-square force was derived by Rosenbluth, *et al.* [40] in the form

$$\frac{1}{\Gamma_a}\left(\frac{\partial f_a}{\partial t}\right)_c = -\frac{\partial}{\partial v_i}\left(f_a \frac{\partial h_a}{\partial v_i}\right) + \frac{1}{2}\frac{\partial^2}{\partial v_i \partial v_j}\left(f_a \frac{\partial^2 g_a}{\partial v_i \partial v_j}\right) \tag{4.1}$$

where $\Gamma_a = 4\pi Z_a^4 e^4 / m_a^2$. In the present work we write the "Rosenbluth potentials"

$$g_a = \sum_b \left(\frac{Z_b}{Z_a}\right)^2 \ln \Lambda_{ab} \int f_b(\boldsymbol{v}') |\boldsymbol{v} - \boldsymbol{v}'| \, d\boldsymbol{v}', \tag{4.2}$$

$$h_a = \sum_b \frac{m_a + m_b}{m_b} \left(\frac{Z_b}{Z_a}\right)^2 \ln \Lambda_{ab} \int f_b(\boldsymbol{v}') |\boldsymbol{v} - \boldsymbol{v}'|^{-1} d\boldsymbol{v}'. \tag{4.3}$$

The functions g_a and h_a, defined by (4.2) and (4.3), can be represented by expansions in Legendre polynomials [10]. Summation is over all species.

Equation (4.1) in (v, θ) coordinates, written in conservative form, is

$$\frac{1}{\Gamma_a}\left(\frac{\partial f_a}{\partial t}\right)_c = \frac{1}{v^2}\frac{\partial G_a}{\partial v} + \frac{1}{v^2 \sin\theta}\frac{\partial H_a}{\partial \theta} \tag{4.4}$$

where

$$G_a = A_a f_a + B_a \frac{\partial f_a}{\partial v} + C_a \frac{\partial f_a}{\partial \theta} \quad \text{and} \quad H_a = D_a f_a + E_a \frac{\partial f_a}{\partial v} + F_a \frac{\partial f_a}{\partial \theta}.$$

The coefficients which involve derivatives of g_a and h_a are defined in [10], [39]. Equation (4.4) is integrated using the method of splitting, or fractional timesteps. We first advance

$$\frac{1}{\Gamma_a}\frac{\partial f_a}{\partial t} = \frac{1}{v^2}\frac{\partial G_a}{\partial v} \tag{4.5}$$

using an implicit difference algorithm and then advance

$$\frac{1}{\Gamma_a}\frac{\partial f_a}{\partial t} = \frac{1}{v^2 \sin\theta}\frac{\partial H_a}{\partial \theta} \tag{4.6}$$

in an analogous manner. Equation (4.5) is differenced as follows:

$$\begin{aligned} \frac{f_{i,j}^{n+1} - f_{i,j}^n}{\Gamma_a \Delta t} &= \frac{A_{i,j+1}^n f_{i,j+1}^{n+1} - A_{i,j-1}^n f_{i,j-1}^{n+1}}{2 v_j^2 \Delta v_j} + \\ &+ \frac{1}{v_j^2}\left[\frac{B_{i,j+1/2}^n (f_{i,j+1}^{n+1} - f_{i,j}^{n+1})}{\Delta v_{j+1/2}} - \frac{B_{i,j-1/2}^n (f_{i,j}^{n+1} - f_{i,j-1}^{n+1})}{\Delta v_{j-1/2}}\right] + \\ &+ \frac{1}{2 v_j^2 \Delta v_j}\left[\frac{C_{i,j+1}^n (f_{i+1,j+1}^n - f_{i-1,j+1}^n)}{2\Delta\theta_i} - \frac{C_{i,j-1}^n (f_{i+1,j-1}^n - f_{i-1,j-1}^n)}{2\Delta\theta_i}\right]. \end{aligned} \tag{4.7}$$

We see that the terms of mixed second derivative type may not be written fully implicitly if we wish to maintain a tri-diagonal form. Equation (4.6) is integrated in a similar manner, with the roles of v and θ reversed. We have also used the ADI algorithm for the solution of the Fokker–Planck equation [9], and we have a version in which equation (4.4) is differenced fully implicitly including the mixed second derivative and the resulting algebraic problem is solved by the ICCG method [41].

4.2. Transport equations. The spatial independent variable for the transport model is $\varrho = (V/2\pi^2 R_0)^{1/2}$, where V is the volume within the flux surface and R_0 is the major radius of the torus. We can consider an arbitrary number of warm ion species, each described by an equation of the form

$$\frac{\partial n_a}{\partial t} = -\frac{1}{\varrho}\frac{\partial}{\partial \varrho}(\varrho \Gamma_a) + \int (S_{bc} + c_b f_b)\, d\boldsymbol{v} \cdot \delta(a, b). \tag{4.8}$$

The term Γ_a is the particle flux for species "a", and depends on the plasma transport model used ([39], [42]); S_{bc} represents the transfer of low energy

particles from a hot species to its corresponding background; c_b is an inverse charge exchange time.

The electron density is determined by quasi-neutrality and $T_e(\varrho, t)$ is governed by

$$\frac{\partial}{\partial t}\left(\tfrac{3}{2} n_e T_e\right) = -\frac{1}{\varrho}\frac{\partial}{\partial \varrho}(rQ_e) - Q_\Delta + \sum_b Q_{eb} - \tfrac{3}{2} n_e T_e/\hat{\tau}_e + \langle J_\varphi E_\varphi \rangle; \tag{4.9}$$

Q_e is the electron energy flux ([39], [42]); Q_Δ represents energy transfer between ions and electrons; Q_{eb} represents heating of electrons by energetic species "b"; $\hat{\tau}_e$ is the electron energy confinement time, and $\langle J_\varphi E_\varphi \rangle$ is the Ohmic heating term where $\langle\ \rangle$ denotes a flux surface average.

The warm ions are all assumed to be at the same temperature ([42]), and their temperature is determined by

$$\frac{\partial}{\partial t}\left(\tfrac{3}{2}\sum_a n_a T_i\right) = -\frac{1}{\varrho}\frac{\partial}{\partial \varrho}(\varrho Q_i) + Q_\Delta + \hat{Q} + \sum_{a,b} Q_{ab} + \tfrac{3}{2} T_i \sum_{a,b} \int (S_{bc} + c_b f_b)\vec{dv}\,\delta(a, b); \tag{4.10}$$

Q_i is the ion energy flux; Q_Δ and $\hat{Q}$ represent energy transfer between particles; Q_{ab} is the heating of species "a" by energetic species "b", and the last term represents the energy transferred from the hot species to the warm plasma because of particle transfer from the energetic species to the plasma.

The form of the flux terms is ([39]):

$$\Gamma_a = \sum_b D_{ab}^d \frac{\partial n_b}{\partial \varrho} + D_a^i \frac{\partial T_i}{\partial \varrho} + D_a^e \frac{\partial T_e}{\partial \varrho}, \tag{4.11}$$

$$Q_i = \sum_b L_b^d \frac{\partial n_b}{\partial \varrho} + L^i \frac{\partial T_i}{\partial \varrho} + L^e \frac{\partial T_e}{\partial \varrho}, \tag{4.12}$$

$$Q_e = \sum_b M_b^d \frac{\partial n_b}{\partial \varrho} + M^i \frac{\partial T_i}{\partial \varrho} + M^e \frac{\partial T_e}{\partial \varrho}, \tag{4.13}$$

where "b" is summed over warm ion species. If we substitute (4.11)–(4.13) into (4.8)–(4.10) we see that we have a coupled system of one-dimensional diffusion equations which are solved by standard implicit difference techniques which are discussed in [43], [44].

In addition to the transport equations (4.8)–(4.10) we have the

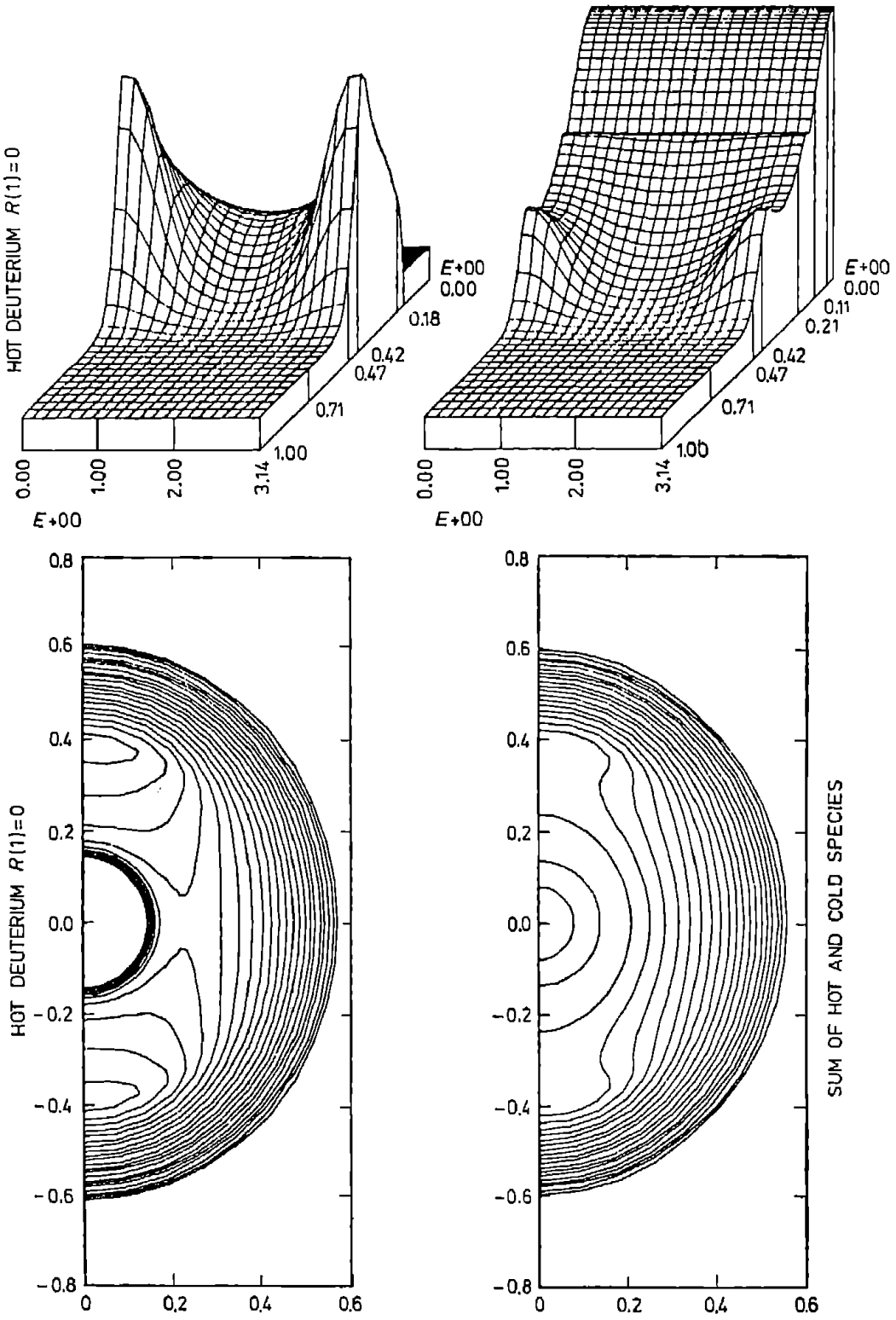

Fig. 1. Distribution function, $f(\varrho, v, \theta)$, versus v and θ at $\varrho = 0$ for hot deuterium (counterstreaming beams) and the sum of hot and cold deuterium. Contour plots of the same distribution function in $(v_\perp\ v_\parallel)$ space

equation for the poloidal magnetic field which is changing in time

$$\frac{\partial \tilde{B}_\varrho}{\partial t} = \frac{c}{R_0}\frac{\partial}{\partial \varrho}\langle RE_\varphi \rangle, \tag{4.14}$$

E_φ is the flux averaged toroidal electric field. Equation (4.14) is solved with (4.8)–(4.10) as part of the transport section of the code.

4.3. Applications. As mentioned earlier the FPT code is used to model the behavior of beam driven Tokamaks ([39]). The code is particularly suitable for studying reactor operation with counterstreaming ion beams (CIT). In this work a simplified transport model is used ([45]). This model has also been applied to counterstreaming deuterium beams in the PDX Tokamak. Fig. 1 shows the distribution function of the hot deuterium plasma formed and also the sum of the hot component and the warm background plasma distribution functions.

References

[1] K. Hain, G. Hain, K. V. Roberts, S. J. Roberts, and W. Köppendörfer, Z. Naturforsch. 15a (1960), 1039.

[2] K. V. Roberts and D. E. Potter, in *Methods in Computational Physics*, Vol. 9, Academic Press, New York 1970, pp. 340–417.

[3] J. Killeen, in *Information Processing 71*, North-Holland Publishing Company, Amsterdam 1972, pp. 1191–1205.

[4] J. U. Brackbill, in *Methods in Computational Physics*, Vol. 16, Academic Press, New York 1976, pp. 1–41.

[5] David Potter, ibid., pp. 43–84.

[6] D. Biskamp, in *Proc. College of Theoretical and Computational Plasma Physics*, Trieste 1977 (IAEA Vienna).

[7] I. Lindemuth and J. Killeen, J. Comput. Phys. 13 (1973), 181.

[8] R. Morse, in *Methods in Computational Physics*, Vol. 9, Academic Press, New York 1970, pp. 213–240.

[9] J. Killeen and K. D. Marx, *The Solution of the Fokker–Planck Equation for a Mirror-Confined Plasma*, in *Methods in Computational Physics*, Vol. 9, Academic Press, New York 1970, pp. 421–489.

[10] J. Killeen, A. A. Mirin, and M. E. Rensink, in *Methods in Computational Physics*, Vol. 16, Academic Press, New York 1976, pp. 389–432.

[11] H. P. Furth, J. Killeen, and M. N. Rosenbluth, Phys. Fluids 6 (1963), 459.

[12] J. Killeen and H. P. Furth, Bull. Amer. Phys. Soc. 6 (1961), 193.

[13] J. Killeen, in *Physics of Hot Plasmas*, edited by B. J. Rye and J. C. Taylor, Plenum, New York 1970, p. 202.

[14] J. E. Crow, J. Killeen, and D. C. Robinson, *Sixth European Conference on Controlled Fusion and Plasma Physics*, Moscow 1973, 269.

[15] D. C. Robinson, J. E. Crow, J. A. Dibiase, A. S. Furzer, and J. Killeen, *The Growth of Resistive Instabilities in a Diffuse Pinch* (1980), to be published.

[16] A. J. L. Verhage, A. S. Furzer, and D. C. Robinson, Nucl. Fusion 18 (1978), 457.

[17] D. C. Robinson, ibid., 18 (1978), 939.
[18] J. Dibiase, Ph. D. Thesis, Univ. of Calif., Davis, UCRL-51591 (1974).
[19] J. Dibiase and J. Killeen, J. Comput. Phys. 24 (1977), 158.
[20] J. A. Dibiase, J. Killeen, D. C. Robinson, D. Schnack, in *Third Topical Conf. on Pulsed High Beta Plasmas (Culham 1975)*, Pergamon Press, Oxford 1976, pp. 283–289.
[21] D. Dobrott, S. C. Prager, and J. B. Taylor, Phys. Fluids 20 (1977), 1850.
[22] J. Killeen and A. I. Shestakov, ibid., 21 (1978), 1746.
[23] A. I. Shestakov, J. Killeen, D. D. Schack, J. Comput. Phys. 46 (1982), 69.
[24] D. Schnack and J. Killeen, in *Theoretical and Computational Plasma Physics*, Trieste 1977, IAEA Vienna 1978, 337–360.
[25] B. V. Waddell, M. N. Rosenbluth, D. A. Monticello, and R. B. White, Nucl. Fusion 16 (1976), 528.
[26] H. R. Hicks, B. Carreras, J. A. Holmes, and B. V. Waddell, ORNL/TM-60966 (1977).
[27] B. V. Waddell, B. Carreras, H. R. Hicks, J. A. Holmes, and D. K. Lee, ORNL/TM-6213 (1978).
[28] B. Carreras, H. R. Hicks, and B. V. Waddell, ORNL/TM-6570 (1978).
[29] G. L. Jahns, M. Soler, B. V. Waddell, J. D. Callen, and H. R. Hicks, Nucl. Fusion 18 (1978), 609.
[30] M. N. Rosenbluth, D. A. Monticello, H. R. Strauss, and R. B. White, Phys. Fluids 19 (1976), 1988.
[31] D. Schnack, Ph. D. Thesis, Univ. of Calif., Davis, UCRL-52399 (1978).
[32] D. Schnack and J. Killeen, *Nonlinear, Two-Dimensional Magnetohydrodynamic Calculations*, J. Comput. Phys. 35 (1980), 110.
[33] D. Schnack and J. Killeen, Nucl. Fusion 19 (1979), 877.
[34] D. D. Schack, J. Killeen, R. A. Gerwin, ibid., 21 (1981), 1447.
[35] D. C. Robinson, Plasma Phys. 13 (1971), 439.
[36] H. P. Furth, P. H. Rutherford, and H. Selberg, Phys. Fluids 16 (1973), 1054.
[37] P. M. Morse and H. Feshbach, *Methods of Theoretical Physics*, McGraw-Hill, New York 1963.
[38] D. L. Jassby, Nucl. Fusion 17 (1977), 309.
[39] A. A. Mirin, J. Killeen, K. D. Marx, and M. E. Rensink, J. Comput. Phys. 23 (1977), 23.
[40] M. N. Rosenbluth, W. M. MacDonald, and D. L. Judd, Phys. Rev. 107 (1957), 1.
[41] M. G. McCoy, A. A. Mirin, A. I. Shestakov and J. Killeen, *Proceedings 9th Conference on Numerical Simulation of Plasmas*, Evanston, Ill., 1980.
[42] J. W. Connor, Plasma Phys. 15 (1973), 765.
[43] J. T. Hogan, in *Methods in Computational Physics*, Vol. 16, Academic Press, New York 1976, pp. 131–165.
[44] M. L. Watkins, M. H. Hughes, P. M. Keeping, K. V. Roberts, and J. Killeen, ibid., pp. 166–210.
[45] D. L. Jassby, R. M. Kulsrud, F. W. Perkins, J. Killeen, K. D. Marx, M. G. McCoy, A. A. Mirin, M. E. Rensink, and C. G. Tull, in *Plasma Physics and Controlled Nuclear Fusion Research 1976*, Vol. II, IAEA Vienna 1977, pp. 435–451.

Presented to the Semester
Computational Mathematics
February 20 – May 30, 1980